Exploring Oscillatory Dysconnectivity Networks in Major Depression during Resting State Using Coupled Tensor Decomposition

Wenya. Liu, Xiulin. Wang, *Student Member, IEEE,* Timo. Hämäläinen, *Senior Member, IEEE* and Fengyu. Cong, *Senior Member, IEEE*

***Abstract*— Dysconnectivity of large-scale brain networks has been linked to major depression disorder (MDD) during resting state. Recent researches show that the temporal evolution of brain networks regulated by oscillations reveals novel mechanisms and neural markers of MDD. Our study applied a novel coupled tensor decomposition model to investigate the dysconnectivity networks characterized by spatio-temporal-spectral modes of covariation in MDD using resting electroencephalography. The phase lag index is used to calculate the functional connectivity within each time window at each frequency bin. Then, two adjacency tensors with the dimension of time $\times$ frequency $\times$ connectivity $\times$ subject are constructed for the healthy group and the major depression group. We assume that the two groups share the same features for group similarity and retain individual characteristics for group differences. Considering that the constructed tensors are nonnegative and the components in spectral and adjacency modes are partially consistent among the two groups, we formulate a double-coupled nonnegative tensor decomposition model. To reduce computational complexity, we introduce the low-rank approximation. Then, the fast hierarchical alternative least squares algorithm is applied for model optimization. After clustering analysis, we summarize four oscillatory networks characterizing the healthy group and four oscillatory networks characterizing the major depression group, respectively. The proposed model may reveal novel mechanisms of pathoconnectomics in MDD during rest, and it can be easily extended to other psychiatric disorders.**

***Index Terms*— Dynamic functional connectivity, coupled tensor decomposition, major depression disorder, oscillatory networks.**

This work was supported by National Natural Science Foundation of China (Grant No.91748105), National Foundation in China (No. JCKY2019110B009 & 2020-JCJQ-JJ-252), the Fundamental Research Funds for the Central Universities [DUT2019 & DUT20LAB303] in Dalian University of Technology in China, and the scholarships from China scholarship Council (No.201706060263). (Corresponding author: Fengyu Cong.)

Wenya Liu is with the School of Biomedical Engineering, Faculty of Electronic Information and Electrical Engineering, Dalian University of Technology, Dalian, 116024, China, Faculty of Information Technology, University of Jyväskylä, Jyväskylä, 40014, Finland, and the Department of Neuroscience and Biomedical Engineering, Aalto University, Espoo, 02150, Finland, (e-mail: wenyaliu0912@foxmail.com).

Xiulin Wang is with Department of Radiology, Affiliated Zhongshan Hospital of Dalian University, Dalian, China, and the School of Biomedical Engineering, Faculty of Electronic Information and Electrical Engineering, Dalian University of Technology, Dalian, 116024, China (e-mail: xiulin.wang@foxmail.com).

Timo Hämäläinen is with Faculty of Information Technology, University of Jyväskylä, Jyväskylä, 40014, Finland (e-mail: timo.t.hamalainen@jyu.fi).

Fengyu Cong is with the School of Biomedical Engineering, Faculty of Electronic Information and Electrical Engineering, Dalian University of Technology, Dalian, 116024, China, Faculty of Information Technology, University of Jyväskylä, Jyväskylä, 40014, Finland, the School of Artificial Intelligence, Faculty of Electronic Information and Electrical Engineering, Dalian University of Technology, 116024, Dalian, China, and the Key Laboratory of Integrated Circuit and Biomedical Electronic System, Liaoning Province. Dalian University of Technology, 116024, Dalian, China (e-mail: cong@dlut.edu.cn).

I. Introduction

MAJOR depression disorder (MDD) is a globally prevalent psychiatric disorder characterized by impairments in affective and cognitive functions [1]. Neuroimaging studies have demonstrated that MDD involves large-scale network dysfunction during resting state, including higher-order intrinsic connectivity networks (ICNs), such as the default mode network (DMN), the dorsal attention network(DAN), the frontoparietal network (FN), and so on [2]. Previous findings correspond to the current understanding of MDD as a network-based disorder [3]. Investigating the neural markers of MDD in pathological networks is valuable for clinical diagnosis and treatment.

Resting state functional connectivity (rsFC) is commonly used to investigate the connectivity structure of MDD [2], [3]. During the past decade, rsFC has been well demonstrated to be dynamic over time relating to states of arousal and information processing [4], [5]. Recently, some resting state functional Magnetic Resonance Imaging (rsfMRI) studies of MDD have reported the abnormal variability of functional connectivity (FC) related to higher-order cognitive functions [6]–[9], but it has not been well verified in electroencephalography (EEG) studies. Besides the dynamic forming and dissolving of FC over time, the spectral modulations also play an important role in network dysfunction in MDD [10]. The electrophysiological oscillation can coordinate brain regions with resonant communications to form a functional network [11]. Different oscillations will exhibit temporally independent FC dynamics that can support frequency-specific information exchange [5], [12]. An increasing amount of researches have investigated altered FC in MDD within different ranges of oscillations using resting EEG, which are most notable in theta, alpha and beta bands [13], [14]. However, most previous studies investigate

the FC during a large range of a predefined frequency band and ignore the exhaustive spectral specificity [10]. The analysis of EEG functional networks requires methods that consider the whole frequency spectrum rather than single frequency bands. Compared with fMRI, EEG has the advantage of high temporal resolution resulting in rich spectral contents, which make it valuable to study the temporal dynamics of frequency-specific functional networks [15]. In this paper, we attended to investigate the abnormal rsFC characterized by spatio-temporal-spectral modes of covariation in MDD.

To evaluate the spatiotemporal dynamics of the resting-state networks (RSNs), matrix decomposition methods, like independent component analysis (ICA), are widely applied to derive the temporal and spatial characteristics of the underlying hidden components or networks in rsfMRI studies [16]. However, matrix decomposition methods will fold some dimensions (like temporal and subject modes) to "artificially flatten" the multiway tensor into a matrix, which will remove the specific information endorsed by higher-order and make it difficult in results interpretation [17]–[20]. Considering the multiway structure of the data, tensor component analysis (TCA) methods have been successfully applied to EEG, MEG and fMRI data under task conditions [20]–[29]. Particularly, to reveal the interactions between different modes, the TCA methods are applied based on the PARAFAC (CP) model or the PARAFAC2 (CP2) model [22], [24]–[26], [28], [29]. However, most of the existing applications are applied under the assumption of spatial consistency, temporal consistency, and spectral consistency, which means that all the subjects will share the same frequency-specific functional networks with the same temporal dynamics. Recently, the coupled canonical polyadic tensor decomposition (coupled CPTD) model is successfully introduced to disentangle different brain states characterized by spatio-temporal-spectral modes of covariation during music listening [30], [31]. For example, Liu et al. applied a double-coupled nonnegative tensor decomposition model to identify the hyper- and hypo-connectivity networks in MDD under music perception. The study constructed two fourth-order tensors with the dimension of time $\times$ frequency $\times$ connectivity $\times$ subject, and the incomplete spatial and spectral consistency were assumed to reveal the shared and unshared oscillatory brain network patterns [31]. In this study, we follow our previously proposed framework in [31], and investigate the altered oscillatory networks in MDD during resting state.

Applying the coupled CPTD model in our study has several advantages. First, it can decompose the multi-block datasets simultaneously and realize the group-level analysis. Second, the resulting rank-1 tensors can reveal the interactions between different modes. Therefore, we can investigate the abnormal brain networks in MDD characterized by spatio-temporal-spectral modes of covariation. Third, by imposing the coupled constraints on the desired modes, it can extract the common and individual features simultaneously, and we can obtain the shared oscillatory networks between the healthy control (HC) group and the MDD group and the unshared oscillatory networks specified in each group. In this study, we proposed a comprehensive framework based on the coupled CPTD model to identify the altered oscillatory networks in MDD during resting state, as shown in Figure 1. The proposed pipeline can be easily extended to applications of other psychiatric disorders.

II. Materials and Methods

A. Data acquisition and preprocessing

The data used in this study are from the Multi-modal Open Dataset for Mental-disorder Analysis (MODMA dataset) which is an open-access dataset [32]. Please refer to [32] for detailed information about the exclusion and inclusion criteria of all participants. Twenty-four MDD subjects and twenty-nine HC subjects participated in the experiment. All the participants signed the informed consent prior to the experiment. The study protocols were approved by the local Ethics Committee for Biomedical Research at the Lanzhou University Second Hospital. All the participants were evaluated by the Patient Health Questionnaire (PHQ-9), Generalized Anxiety Disorder (GAD-7), and Pittsburgh Sleep Quality Index (PSQI). Table I showed the mean and standard deviations (SD) of age, education, PHQ-9, GAD-7, PSQI and gender about two groups. The statistical analysis of age, education, PHQ-9, GAD-7 and PSQI was tested by the two-sample t-test, and the statistical analysis of gender was tested by the chi-squared test.

The EEG signals were recorded by a 128-channel HydroCel Geodesic Sensor Net. Five minutes eye-closed resting state EEG signals were collected with a sampling frequency of $fs = 250$ Hz and a reference of Cz. We preprocessed the data using EEGLAB toolbox [33]. The EEG signals were re-referenced with the average reference and then filtered to 1-40 Hz with the FIR band-pass filter. ICA was applied to remove the artifacts caused by eye movements, and the bad channels were interpolated by spherical interpolations. We visually inspected the signals. To keep the continuousness of the data, we rejected the bad time intervals with large segments. Aftering the final visual inspection and the removal of bad time intervals, the length of the remaining clean data of two MDD patients and five HC subjects were shorter than 3 minutes. To keep the even and sufficient length of the EEG data of all subjects, those seven participants were excluded. After preprocessing, we obtained the three-minute EEG data with twenty-two MDD subjects and twenty-four HC subjects for further analysis.

TABLE I: Means and standard deviations of age, gender, education and clinical measures for HC group and MDD group

	HC group		MDD group		p-value
	Mean	SD	Mean	SD	
Age	32.9	9.1	30.4	9.6	>0.05
Education	15.8	2.5	13.5	3.6	>0.05
PHQ-9	2.5	1.8	18.2	3.6	<0.01
GAD-7	1.9	2.1	13.4	5.2	<0.01
PSQI	4.1	2.3	12.4	4.4	<0.01
Gender	9females, 15 males		10 females, 12 males		>0.05

Abbreviations: HC, healthy controls; MDD, major depression disorder; SD, standard deviations; PHQ-9, Patient Health Questionnaire; GAD-7, Generalized Anxiety Disorder; PSQI, Pittsburgh Sleep Quality Index.

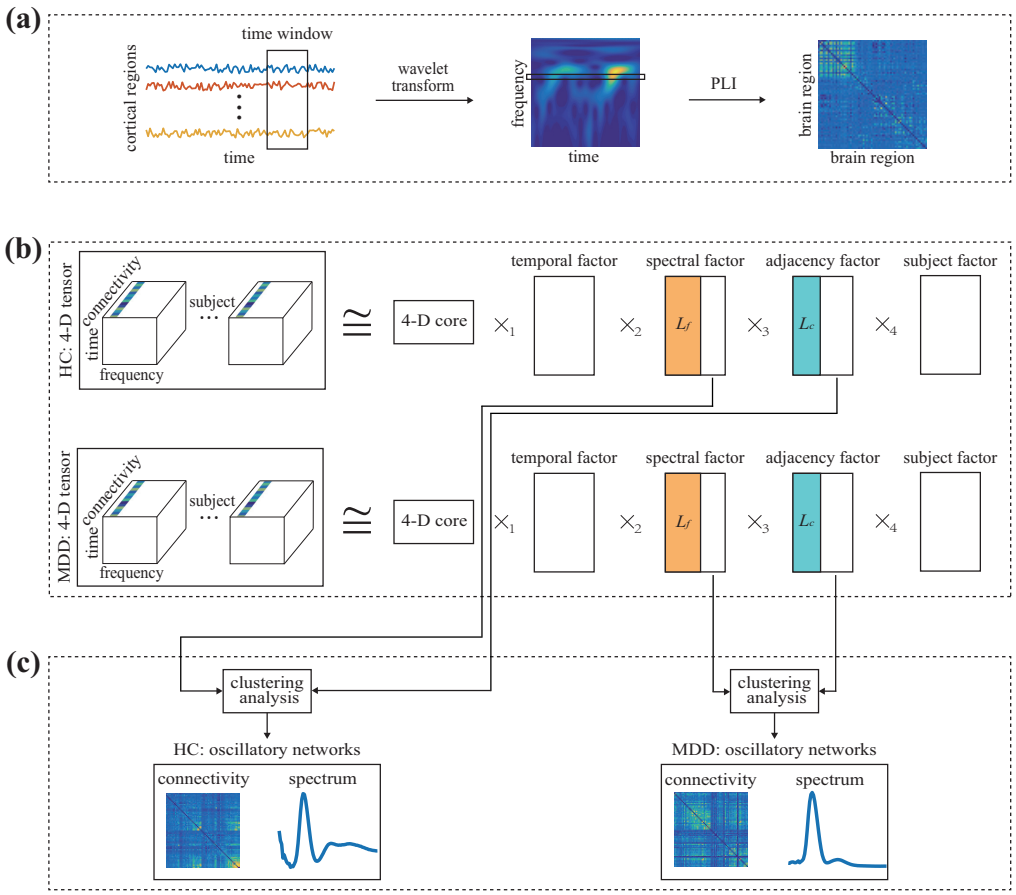

Fig. 1: Diagram of the analysis pipeline. (a) Adjacency matrix construction in each time window and at each frequency bin. After source reconstruction, the cortical signals were segmented by overlapping time windows, and wavelet transform was applied for each time course within each time window. The phase lag index was used to obtain the adjacency matrix for each time window and each frequency bin. (b) Adjacency tensor construction and decomposition. A 4-D adjacency tensor was constructed for each group with the dimension of time × frequency × connectivity × subject, and coupled tensor decomposition was implemented with coupled constraints in spectral and adjacency modes. The 4-D core tensor is superdiagonal with values of 1. (c) The identification of oscillatory networks specified for each group.

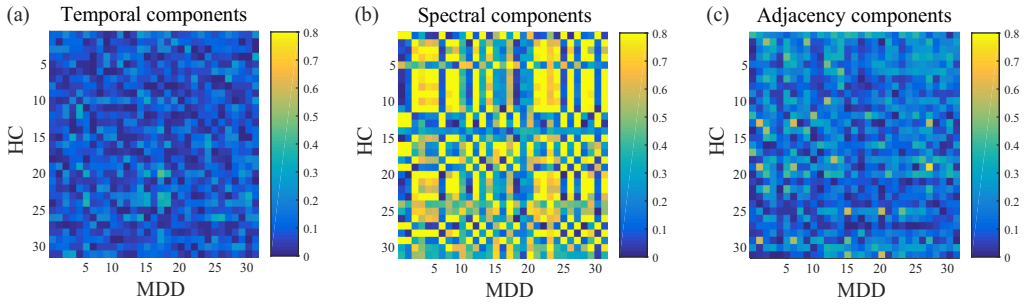

Fig. 2: The correlation maps of (a) temporal components, (b) spectral components and (c) adjacency components between the HC group and the MDD group. The components are extracted by unconstrained CP decomposition on each block tensor of each group.

B. Source reconstruction

We performed source localization with the open-source Brainstorm software [34]. The cortical source currents were estimated from the EEG recordings by solving two distinct modeling problems: forward modeling of head tissues and sensor characteristics and source modeling of source estimation. For forward modeling, the symmetric boundary element method (BEM) from the open-source software OpenMEEG was applied with the MNI-ICBM152 template to compute the volume-conductor model, and the source space was restricted to the cortical surface with a grid of 15000 vertices. For source modeling, we applied the weighted minimum norm estimate (wMNE) method. Because it was well demonstrated

that wMNE could minimize spurious phase interactions by addressing the volume conduction problem and provide better performance in estimating large-scale functional connectivity networks [35], [36]. The current source orientations were constrained normal to the cortical surface, and a depth weighting algorithm was used to compensate for any bias of superficial sources estimation. The regularization parameter was set as 0.1 to reduce the sensitivity to noise. Then, the cortex was parcellated into 68 anatomical regions (34 in each hemisphere) with the Desikan–Killiany atlas [37]. The first principal component of the principal component analysis (PCA) decomposition performed on each brain region was used as the representative time series to calculate pair-wise functional connectivity.

C. Functional connectivity

We calculate the all-to-all whole-brain FC by the phase lag index (PLI) method for the following advantages of PLI [38]. First, phase relations act as a mechanistic role supporting interactions between neuronal groups, and PLI can measure the phase relations between two signals [39]. Second, phase synchronization methods combining with source localization by wMNE have better performance in the estimation of large-scale FC [35]. Third, the PLI method can diminish bias from common sources by discarding zero-lag phase differences manifested by signal leakage.

We represent the reconstructed source signals as $X \in \mathbb{R}^{n_t \times n_s}$, where n_t and n_s represent the number of time points and the number of cortical brain regions, respectively. We segment the source data X in the temporal dimension by a sliding window with the window length of 3 seconds and the overlap of 2 seconds, causing $T = 178$ segmented data $X_t \in \mathbb{R}^{3fs \times n_s}, t = 1, 2, ..., T$. Then, continuous wavelet transform with Morlet wavelets is applied on each segmented data X_t with 0.5 Hz frequency bin, resulting in $F = 59$ frequency points for each time series in X_t. For brain region i and time window t, the complex time-frequency representations are denoted as $P_{i,t} \in \mathbb{R}^{3fs \times F}$. We can obtain the instantaneous phases for brain region i, time window t and frequency f by

$$\varphi_{i,t}(f) = \arctan \frac{imag(P_{i,t}(f))}{real(P_{i,t}(f))}, \tag{1}$$

where $imag()$ and $real()$ represent the imaginary part and the real part of a complex value, respectively.

Then, we can compute the PLI index between brain regions i and j in time window t at frequency f as follows:

$$PLI_{i,j}(t, f) = \left| \langle sign(\varphi_{i,t}(f) - \varphi_{j,t}(f)) \rangle \right|, \tag{2}$$

where $|\cdot|$ means the absolute value, and $\langle \cdot \rangle$ means the sum average value. After calculating all pairs of PLI values, we can construct two adjacency tensors, $\boldsymbol{\mathcal{X}}^{\text{HC}} \in \mathbb{R}^{T \times F \times N \times S_{\text{HC}}}$ for the HC group and $\boldsymbol{\mathcal{X}}^{\text{MDD}} \in \mathbb{R}^{T \times F \times N \times S_{\text{MDD}}}$ for the MDD group. $N = n_s(n_s - 1)/2 = 2278$ represents the number of connections according to the Desikan–Killiany atlas. S_{HC} and S_{MDD} denote the number of subjects in the HC group and the MDD group, respectively. Please note that the constructed tensors are nonnegative, and the value of each element in two tensors is constrained to [0, 1] due to the computation of PLI index.

D. The coupled tensor decomposition

1) The nonnegative and double-coupled constraints: The constructed tensors are concatenated by all pairs of FC strengths (vary from 0 to 1) along temporal, spectral and subject dimensions, causing two nonnegative tensors. Therefore, we impose nonnegative constraints on all the components for each mode, and the derived nonnegative components represent the time envelope, spectrum, connected strength and subject contribution, respectively [30].

In our study, we impose double-coupled constraints on the spectral mode and the adjacency mode. We assume that the resting state oscillatory networks are partially altered in MDD. The two groups can arouse the same functional networks under the same condition and also retain individual functional networks characterizing group differences. We applied unconstrained CP decomposition on each tensor and calculated the correlation maps of the temporal, spectral and adjacency components between two groups, respectively, as shown in Fig 2. The temporal components have a lower correlation between the two groups, and the temporal dynamics are not identical under a task-free condition. According to Fig 2, we couple the different numbers of components in spectral and adjacency modes.

2) The double-coupled nonnegative tensor decomposition: Given a forth-order tensor $\boldsymbol{\mathcal{X}} \in \mathbb{R}^{I_1 \times I_2 \times I_3 \times I_4}$, it can be decomposed into R rank-1 tensors with the general CP decomposition by solving the following minimization problem:

$$\mathcal{J}(\boldsymbol{u}^{(n)}) = \|\boldsymbol{\mathcal{X}} - \sum_{r=1}^{R} \boldsymbol{u}^{(1)} \circ \boldsymbol{u}^{(2)} \circ \boldsymbol{u}^{(3)} \circ \boldsymbol{u}^{(4)}\|_F^2, \tag{3}$$

where $\sum_{r=1}^{R} \boldsymbol{u}^{(1)} \circ \boldsymbol{u}^{(2)} \circ \boldsymbol{u}^{(3)} \circ \boldsymbol{u}^{(4)} = [\![\boldsymbol{U}^{(1)}, \boldsymbol{U}^{(2)}, \boldsymbol{U}^{(3)}, \boldsymbol{U}^{(4)}]\!]$, $\| \cdot \|_F$ denotes the Frobenius norm, and $\circ$ denotes the vector outer product. $\boldsymbol{u}_r^{(n)}$ denotes the rth component of factor matrices $\boldsymbol{U}^{(n)}$, $n = 1, 2, 3, 4$, and R is the number of rank-1 tensors. In our study, for the two forth-order tensors $\boldsymbol{\mathcal{X}}^{\text{HC}} \in \mathbb{R}^{W \times F \times N \times S_{\text{HC}}}$ and $\boldsymbol{\mathcal{X}}^{\text{MDD}} \in \mathbb{R}^{W \times F \times N \times S_{\text{MDD}}}$, to reduce the computational load for further analysis, we firstly applied the low-rank approximation with (3) using the alternating least squares (ALS, [40]) algorithm. Then, we can get the low-rank approximation as $\boldsymbol{\mathcal{X}}^{\text{HC}} \simeq \tilde{\boldsymbol{\mathcal{X}}}^{\text{HC}} = [\![\tilde{\boldsymbol{U}}^{(1)}, \tilde{\boldsymbol{U}}^{(2)}, \tilde{\boldsymbol{U}}^{(3)}, \tilde{\boldsymbol{U}}^{(4)}]\!]$ and $\boldsymbol{\mathcal{X}}^{\text{MDD}} \simeq \tilde{\boldsymbol{\mathcal{X}}}^{\text{MDD}} = [\![\tilde{\boldsymbol{V}}^{(1)}, \tilde{\boldsymbol{V}}^{(2)}, \tilde{\boldsymbol{V}}^{(3)}, \tilde{\boldsymbol{V}}^{(4)}]\!]$.

We want to impose the nonnegative constraints and the double-coupled constraints on spectral (mode-2) and adjacency (mode-3) modes, and this can be formulated as a double-coupled nonnegative tensor decomposition (DC-NTD) model, which can be solved by minimizing the following objective function:

$$\begin{aligned} \mathcal{J}(\boldsymbol{u}_r^{(n)}, \boldsymbol{v}_r^{(n)}) = &\|\tilde{\boldsymbol{\mathcal{X}}}^{\text{HC}} - \sum_{r=1}^{R_{\text{HC}}} \boldsymbol{u}_r^{(1)} \circ \boldsymbol{u}_r^{(2)} \circ \boldsymbol{u}_r^{(3)} \circ \boldsymbol{u}_r^{(4)}\|_F^2 \\ &+ \|\tilde{\boldsymbol{\mathcal{X}}}^{\text{MDD}} - \sum_{r=1}^{R_{\text{MDD}}} \boldsymbol{v}_r^{(1)} \circ \boldsymbol{v}_r^{(2)} \circ \boldsymbol{v}_r^{(3)} \circ \boldsymbol{v}_r^{(4)}\|_F^2 \end{aligned} \tag{4}$$

$$\text{s.t. } \boldsymbol{u}_r^{(2)} = \boldsymbol{v}_r^{(2)} (r \le L_f), \boldsymbol{u}_r^{(3)} = \boldsymbol{v}_r^{(3)} (r \le L_c),$$

where R_{HC} and R_{MDD} are the ranks of tensors $\tilde{\boldsymbol{\mathcal{X}}}^{\text{HC}}$ and $\tilde{\boldsymbol{\mathcal{X}}}^{\text{HC}}$. $\boldsymbol{u}_r^{(n)}$ and $\boldsymbol{v}_r^{(n)}$ are the rth components of the mode-n actor matrices $\boldsymbol{U}^{(n)}$ and $\boldsymbol{V}^{(n)}$, $n = 1, 2, 3, 4$, for the HC group and the MDD group, respectively. L_f and L_c denote the number of components coupled in spectral and adjacency modes, and $L_{f,c} \leq \min(R_{\text{HC}}, R_{\text{MDD}})$.

We applied the fast hierarchical alternative least squares (FHALS) algorithm to optimize the DC-NTD problem in (4). Besides the advantages of high accuracy and easy realization in optimization, the FHALS algorithm can also reduce the computational load for large-scale tensors, and it has been effectively applied to a number of (coupled) tensor decomposition problems regarding nonnegative matrices and tensors [30], [31], [41], [42]. The minimization problem in (4) can be converted into $\max(R_{\text{HC}}, R_{\text{MDD}})$ rank-1 subproblems through the FHALS algorithm. The rth subproblem can be denoted as follows:

$$\begin{aligned}\min \mathcal{J}_r(\boldsymbol{u}_r^{(n)}, \boldsymbol{v}_r^{(n)}) = \|\tilde{\boldsymbol{\mathcal{Y}}}_r^{\text{HC}} - \boldsymbol{u}_r^{(1)} \circ \boldsymbol{u}_r^{(2)} \circ \boldsymbol{u}_r^{(3)} \circ \boldsymbol{u}_r^{(4)}\|_F^2 \\ + \|\tilde{\boldsymbol{\mathcal{Y}}}_r^{\text{MDD}} - \boldsymbol{v}_r^{(1)} \circ \boldsymbol{v}_r^{(2)} \circ \boldsymbol{v}_r^{(3)} \circ \boldsymbol{v}_r^{(4)}\|_F^2,\end{aligned} \tag{5}$$

where $\tilde{\boldsymbol{\mathcal{Y}}}_r^{\text{HC}} \doteq \tilde{\boldsymbol{\mathcal{X}}}^{\text{HC}} - \sum_{k \neq r}^{R_{\text{HC}}} \boldsymbol{u}_k^{(1)} \circ \boldsymbol{u}_k^{(2)} \circ \boldsymbol{u}_k^{(3)} \circ \boldsymbol{u}_k^{(4)}$ and $\tilde{\boldsymbol{\mathcal{Y}}}_r^{\text{MDD}} \doteq \tilde{\boldsymbol{\mathcal{X}}}^{\text{MDD}} - \sum_{k \neq r}^{R_{\text{MDD}}} \boldsymbol{v}_k^{(1)} \circ \boldsymbol{v}_k^{(2)} \circ \boldsymbol{v}_k^{(3)} \circ \boldsymbol{v}_k^{(4)}$ are the kth rank-1 tensor in each group. This subproblem can be solved sequentially and iteratively. For example, to get $\boldsymbol{u}_r^{(n)}$, we need to calculate the gradient $\mathcal{J}_r(\boldsymbol{u}_r^{(n)}, \boldsymbol{v}_r^{(n)})$ with respect to $\boldsymbol{u}_r^{(n)}$ as follows:

$$\frac{\partial \mathcal{J}_r(\boldsymbol{u}_r^{(n)}, \boldsymbol{v}_r^{(n)})}{\partial \boldsymbol{u}_r^{(n)}} = -2\tilde{\boldsymbol{Y}}_{r,(n)}^{\text{HC}} \left[\boldsymbol{u}_r\right]^{\odot_{-n}} + 2\boldsymbol{u}_r^{(n)} \left[\boldsymbol{u}_r{}^T \boldsymbol{u}_r\right]^{\circledast_{-n}}, \tag{6}$$

where $\odot$ and $\circledast$ denote the Khatri-Rao product and Hadamard (element-wise) product. where $\tilde{\boldsymbol{Y}}_{r,(n)}^{\text{HC}}$ is the mode-n matricization of $\tilde{\boldsymbol{\mathcal{Y}}}_r^{\text{HC}}$. $\left[\boldsymbol{u}_r\right]^{\odot_{-n}} = \boldsymbol{u}_r^{(4)} \odot \cdots \odot \boldsymbol{u}_r^{(n+1)} \odot \boldsymbol{u}_r^{(n-1)} \odot \cdots \odot \boldsymbol{u}_r^{(1)}$ and $\left[\boldsymbol{u}_r{}^T \boldsymbol{u}_r\right]^{\circledast_{-n}} = \left([\boldsymbol{u}_r]^{\odot_{-n}}\right)^T [\boldsymbol{u}_r]^{\odot_{-n}}$. Specially, for $r \leq L_f$, $n = 2$ and $r \leq L_c$, $n = 3$, the gradient should be represented as:

$$\begin{aligned}\frac{\partial \mathcal{J}_r(\boldsymbol{u}_r^{(n)}, \boldsymbol{v}_r^{(n)})}{\partial \boldsymbol{u}_r^{(n)}} = &-2\tilde{\boldsymbol{Y}}_{r,(n)}^{\text{HC}} \left[\boldsymbol{u}_r\right]^{\odot_{-n}} + 2\boldsymbol{u}_r^{(n)} \left[\boldsymbol{u}_r{}^T \boldsymbol{u}_r\right]^{\circledast_{-n}} \\ &- 2\tilde{\boldsymbol{Y}}_{r,(n)}^{\text{MDD}} \left[\boldsymbol{v}_r\right]^{\odot_{-v}} + 2\boldsymbol{v}_r^{(n)} \left[\boldsymbol{v}_r{}^T \boldsymbol{v}_r\right]^{\circledast_{-n}}.\end{aligned} \tag{7}$$

Then, let the gradient in (6) and (7) be zero, we can get the solution of $\boldsymbol{u}_r^{(n)}$ via hierarchical alternative least squares (HALS) as:

$$\boldsymbol{u}_r^{(n)} = \tilde{\boldsymbol{Y}}_{r,(n)}^{\text{HC}} \left[\boldsymbol{u}_r\right]^{\odot_{-n}} / \left[\boldsymbol{u}_r{}^T \boldsymbol{u}_r\right]^{\circledast_{-n}} \tag{8}$$

or

$$\begin{aligned}\boldsymbol{u}_r^{(n)} = &\tilde{\boldsymbol{Y}}_{r,(n)}^{\text{HC}} \left[\boldsymbol{u}_r\right]^{\odot_{-n}} / \left[\boldsymbol{u}_r{}^T \boldsymbol{u}_r\right]^{\circledast_{-n}} + \\ &\tilde{\boldsymbol{Y}}_{r,(n)}^{\text{MDD}} \left[\boldsymbol{v}_r\right]^{\odot_{-n}} / \left[\boldsymbol{v}_r{}^T \boldsymbol{v}_r\right]^{\circledast_{-n}}\end{aligned} \tag{9}$$

when $r \leq L_f$, $n = 2$ and $r \leq L_c$, $n = 3$.

For the solutions via FHALS, we set $\tilde{\boldsymbol{Y}}_{r,(n)}^{\text{HC}} = \tilde{\boldsymbol{U}}^{(n)} \left[\tilde{\boldsymbol{U}}^{\odot_{-n}}\right]^T - \boldsymbol{U}^{(n)} [\boldsymbol{U}^{\odot_{-n}}]^T + \boldsymbol{u}_r^{(n)} [\boldsymbol{u}_r^{\odot_{-n}}]^T$ and $\tilde{\boldsymbol{Y}}_{r,(n)}^{\text{MDD}} = \tilde{\boldsymbol{V}}^{(n)} \left[\tilde{\boldsymbol{V}}^{\odot_{-n}}\right]^T - \boldsymbol{V}^{(n)} [\boldsymbol{V}^{\odot_{-n}}]^T + \boldsymbol{v}_r^{(n)} [\boldsymbol{v}_r^{\odot_{-n}}]^T$. Then. we can rewrite (8) and (9) as:

$$\boldsymbol{u}_r^{(n)} = \boldsymbol{u}_r^{(n)} + \left[\tilde{\boldsymbol{U}}^{(n)} \tilde{\boldsymbol{\Gamma}}_r^{(n)} - \boldsymbol{U}^{(n)} \boldsymbol{\Gamma}_r^{(n)}\right] / \boldsymbol{\Gamma}_{(r,r)}^{(n)} \tag{10}$$

and

$$\begin{aligned}&\boldsymbol{u}_r^{(n)} = \boldsymbol{v}_r^{(n)} = \boldsymbol{u}_r^{(n)} + \\ &\left[\tilde{\boldsymbol{U}}^{(n)} \tilde{\boldsymbol{\Gamma}}_r^{(n)} - \boldsymbol{U}^{(n)} \boldsymbol{\Gamma}_r^{(n)} + \tilde{\boldsymbol{V}}^{(n)} \tilde{\boldsymbol{\Lambda}}_r^{(n)} - \boldsymbol{V}^{(n)} \boldsymbol{\Lambda}_r^{(n)}\right] / \left[\boldsymbol{\Gamma}_{(r,r)}^{(n)} + \boldsymbol{\Lambda}_{(r,r)}^{(n)}\right]\end{aligned} \tag{11}$$

when $r \leq L_f$, $n = 2$ and $r \leq L_c$, $n = 3$, where $\tilde{\boldsymbol{\Gamma}}^{(n)} = [\tilde{\boldsymbol{U}}^T \boldsymbol{U}]^{\circledast_{-n}}$, and $\tilde{\boldsymbol{\Lambda}}^{(n)} = [\tilde{\boldsymbol{V}}^T \boldsymbol{V}]^{\circledast_{-n}}$. Analogously, except $r \leq L_f$, $n = 2$ and $r \leq L_c$, $n = 3$, we can obtain the learning rule of $\boldsymbol{v}_r^{(n)}$ as follows:

$$\boldsymbol{v}_r^{(n)} = \boldsymbol{v}_r^{(n)} + \left[\tilde{\boldsymbol{V}}^{(n)} \tilde{\boldsymbol{\Lambda}}_r^{(n)} - \boldsymbol{V}^{(n)} \boldsymbol{\Lambda}_r^{(n)}\right] / \boldsymbol{\Lambda}_{(r,r)}^{(n)}. \tag{12}$$

To keep the nonnegativity of the components, we applied the "half-rectifying" nonlinear projection. In each subproblem, $\boldsymbol{u}_r^{(n)}$ and $\boldsymbol{v}_r^{(n)}$ are updated successively via (10), (11) and (12). The $\max(R_{\text{HC}}, R_{\text{MDD}})$ subproblems are optimized alternatively one after another until convergence. We summarize the DC-NTD-FHALS algorithm in **Algorithm** 1.

Algorithm 1: DC-NTD-FHALS algorithm

Input: $\boldsymbol{\mathcal{X}}^{\text{HC}}$, $\boldsymbol{\mathcal{X}}^{\text{MDD}}$, L_f, L_c, R_{HC}, R_{MDD}

Initialization: $\boldsymbol{U}^{(n)}$, $\boldsymbol{V}^{(n)}$, $n = 1, 2, 3, 4$

Calculate $\tilde{\boldsymbol{U}}^{(n)}$, $\tilde{\boldsymbol{V}}^{(n)}$, $n = 1, 2, 3, 4$ via unconstrained ALS

while *unconvergence* **do**

  for $n = 1, 2, \cdots, 4$ **do**

    for $r = 1, 2, \cdots max(R_{HC}, R_{MDD})$ **do**

      Update $\boldsymbol{u}_r^{(n)}$, $\boldsymbol{v}_r^{(n)}$ via (10), (11) and (12)

    end

  end

end

Output: $\boldsymbol{U}^{(n)}$, $\boldsymbol{V}^{(n)}$, $n = 1, 2, 3, 4$

3) Parameter settings: For the implementation of the DC-NTD-FHALS algorithm, we need to select the number of extracted components R_{HC} and R_{MDD} for two tensors $\boldsymbol{\mathcal{X}}^{\text{HC}}$ and $\boldsymbol{\mathcal{X}}^{\text{MDD}}$, and the number of coupled components L_f and L_c in the spectral and adjacency modes. For R_{HC} and R_{MDD}, we matricized the tensors $\boldsymbol{\mathcal{X}}^{\text{HC}}$ and $\boldsymbol{\mathcal{X}}^{\text{MDD}}$ along the spectral mode separately. Then, we performed PCA and select the number of components according to 95% explained variance. In our study, we set $R_{HC} = R_{MDD} = 31$. Please note that we use the same number of components in low-rank approximation. There are no common methods to select the coupled modes and the number of coupled components because of different data characteristics regarding different applications. Following our previous studies [30], [31], we performed CP decomposition on each tensor and calculated the correlation maps of temporal components, spectral components and adjacency components between the HC group and the MDD group, as shown in Figure 2. According to the correlation maps, we impose the coupled constraints in spectral and adjacency

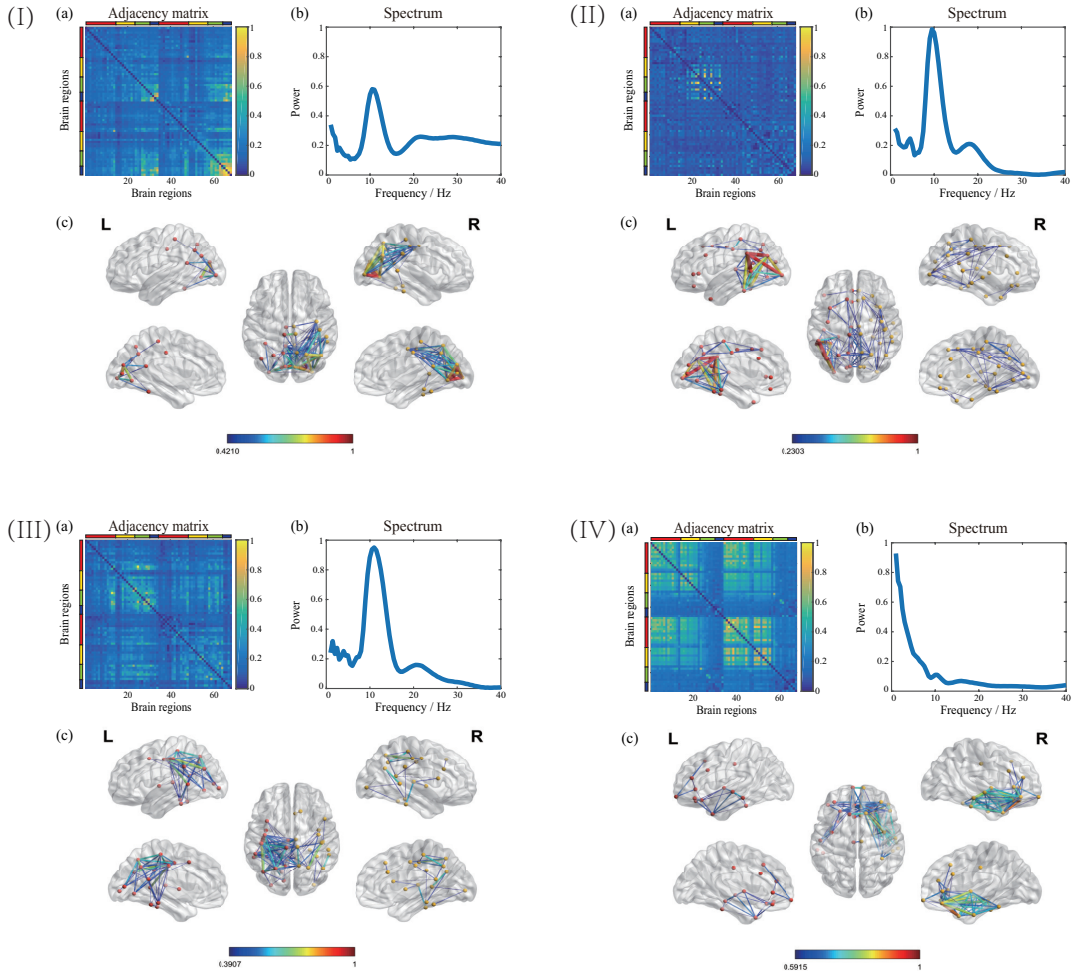

Fig. 3: Four oscillatory networks specified in the HC group. (a) Adjacency matrix representation of the network. The 68 brain regions are ordered from the left hemisphere to the right hemisphere. Within each hemisphere, the brain regions are arranged in the order of frontal lobe, temporal lobe, parietal lobe, and occipital lobe, as indicated in red, yellow, green, and blue color, respectively. Within each lobe, the brain regions are ordered according to their y-location from anterior regions to posterior regions. (b) The spectral component of the network. (c) Cortical space representation of the network in lateral, medial and dorsal view.

modes, and we set the number of coupled components in the spectral mode $L_f = 25$ and the number of coupled components in the adjacency mode $L_c = 9$.

For the initialization of the factors in each mode, we applied the uniformly distributed pseudorandom numbers. We set two termination criteria for the iterations. The change of the tensor fitting is smaller than $\varepsilon = 1e-6$, or the number of iterations is up to 1000.

III. Results

We implemented the low-rank DC-NTF-FHALS algorithm 50 times, and the average running time was 9949 seconds. For the individual networks in the HC group from 50 times implementations of the proposed algorithm, we performed PCA to determine the number of clusters according to 95% explained variance, and then the k-means clustering method was applied to obtain the stable networks extracted by the low-rank DC-NTF-FHALS algorithm. The same clustering procedure was also performed for the MDD group.

We clustered four oscillatory networks from the individual networks in the HC group, which also represent the hypoconnectivity networks in MDD, as shown in Figure 3. Those hypoconnectivity networks mean that they are activated in the HC group but not in the MDD group. Figure 3I-III were alpha rhythm modulated networks. Figure 3I showed a right visual network modulated by upper-alpha rhythms. Figure 3II showed a left hemisphere dominated temporoparietal network (TPN) with a 10 Hz oscillatory peak. This dysconnectivity network converges in the temporoparietal junction (TPJ), which plays a crucial role in controlling higher-order cognition during the task-free state. Figure 3III showed a sensorimotor network (SMN) which has a great clinical significance in various neuropsychiatric disorders. A bilateral frontotemporal network(FTN) was identified to be modulated by delta band, which was related to various brain diseases, as shown in Figure 3IV.

We also clustered four oscillatory networks specified in the MDD group, which represented the hyperconnectivity net-

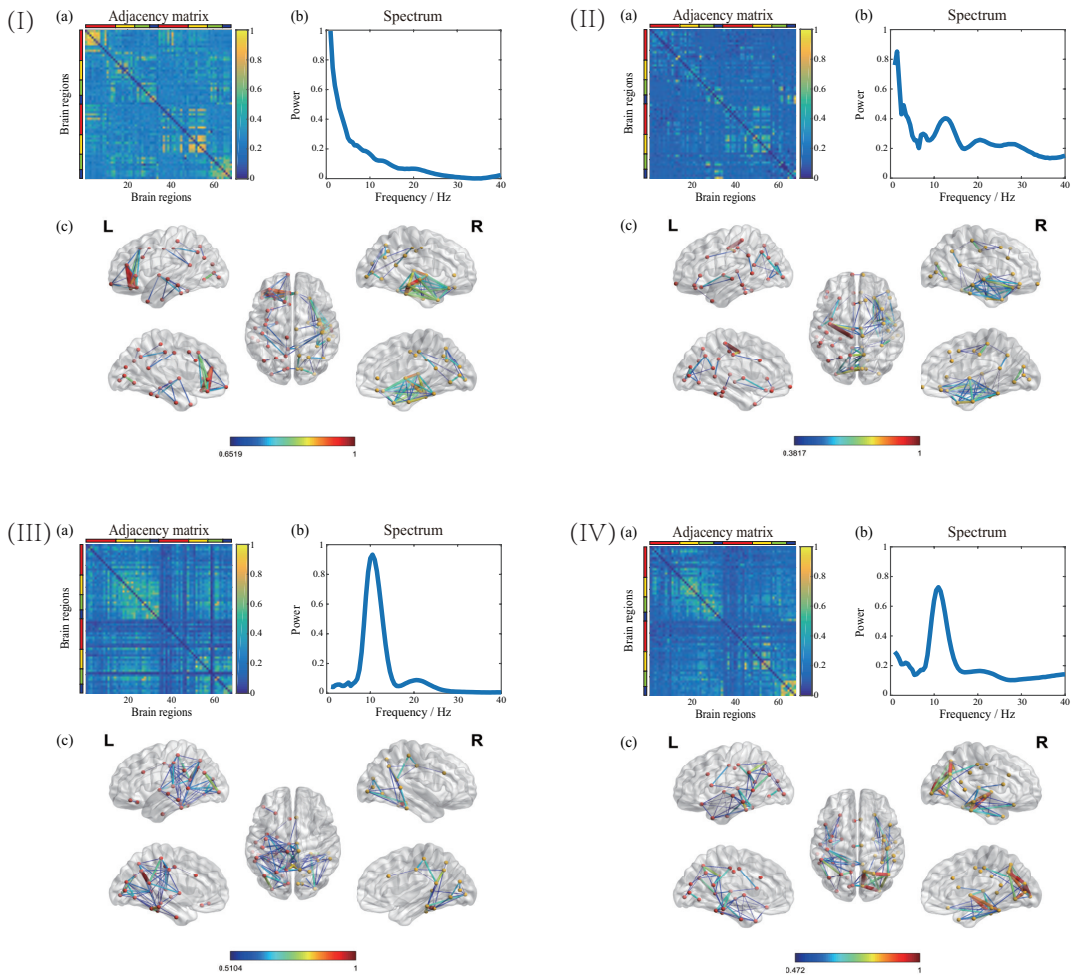

Fig. 4: Four oscillatory networks specified in the MDD group. (a) Adjacency matrix representation of the network. The 68 brain regions are ordered from the left hemisphere to the right hemisphere. Within each hemisphere, the brain regions are arranged in the order of frontal lobe, temporal lobe, parietal lobe, and occipital lobe, as indicated in red, yellow, green, and blue color, respectively. Within each lobe, the brain regions are ordered according to their y-location from anterior regions to posterior regions. (b) The spectral component of the network. (c) Cortical space representation of the network in lateral, medial and dorsal view.

works in MDD, as shown in Figure 4. Those hyperconnectivity networks mean that they are activated in the MDD group but not in the HC group. Figure 4I and Figure 4II indicated delta oscillatory networks. Figure 4I showed a left prefrontal and right auditory network, and Figure 4II showed a right FTN. The networks shown in Figure 4III and Figure 4IV were modulated by late alpha oscillations. Figure 4III showed a posterior network, which involved key areas of DMN, including posterior cingulate cortex (PCC), precuneus and isthmus cingulate cortex (ICC). Figure 4IV represented a DAN-related network which also includes functionally connected visual cortex.

IV. Discussion

In this study, we proposed a comprehensive framework based on coupled tensor decomposition to investigate the hyperconnectivity and hypoconnectivity oscillatory networks in MDD using resting EEG. The applied method has been well demonstrated by synthetic data and real data in our previous study [31]. Our approach is completely data-driven without any assumptions on predefined frequency bands and selections of regions of interest, which can allow us to explore the whole-brain spatial couplings via synchronized oscillations of the rhythmic brain on the exhaustive spectrum contents. This study identified four hyperconnectivity networks and four hypoconnectivity networks modulated by different oscillations. To the best of our knowledge, this study is the first attempt to investigate the frequency-specific dysconnectivity networks in MDD based on the coupled tensor decomposition method using resting EEG.

The oscillatory networks specified in the HC group also represent the hypoconnectivity networks in the MDD group which means that they are normally engaged in the HC group but are underactive in the MDD group. The hyperconnectivity networks specified in the MDD group denote that they are overactive in MDD. Among those dysconnectivity networks, three networks are related to sensory cortex systems, including the visual network in Figure 3I, the SMN in Figure 3III and

the auditory network in Figure 4I. The auditory and visual networks are important ICNs during resting state, which may serve as effective neural markers in MDD [2], [43]–[47]. The anomalous visual and auditory networks may indicate the deficit in processing and integrating audio and visual information in MDD. The abnormalities of visual and auditory networks are widely reported in previous task-based studies. However, few resting state studies investigate the dysfunctions of visual and auditory networks, which should be considered in terms of functional and neuropathological underpinnings [43], [44], [47]. Dysfunction in SMN has been implicated in various neuropsychiatric disorders underlying the sensorimotor functions [48]–[50]. Researches have reported that MDD was characterized by the abnormal spatiotemporal structure of SMN during resting state, and our findings are well in accord with previous studies [50], [51]. We also found some dysconnectivity networks related to higher-order cognitive functions. Figure 3II relates to the left TPN, including strong connections between the inferior parietal cortex, supramarginal gyrus and banks of the superior temporal sulcus. The key regions involve the left temporoparietal junction (LTPJ) area, which is a key node for the integration of internal and external information relating to processing language and semantics [52]–[54]. The LTPJ is also necessary for the representation of mental states [55], [56]. The dysconnectivity of the LTPJ may indicate the deficit in language-related functions and the inference of others' intention in MDD [52], [54], [55]. We identified the dysconnectivity of the FTN, which is bilaterally activated in the HC group (Figure 3IV) and unilaterally activated in the MDD group (Figure 4II). The dysfunction of frontotemporal regions is the main cause of frontotemporal dementia (FTD), which affects emotion regulation, memory and language processing, and MDD is commonly an early stage of FTD [57], [58]. Our findings potentially indicate that MDD patients may have a risk of developing FTD. Figure 4III showed a posterior network that involves the key areas of DMN, including PCC, ICC and precuneus. The posterior DMN has been implicated in visual processing, motor planning, memory retrieval and self-perception, and altered DMN connectivity may change the way a person perceives events and their social and moral reasoning [59]. The dysconnectivity of DMN is widely reported in MDD during resting state [60], [61]. Increased DMN connectivity is associated with rumination leading to negative and self-referential thoughts [31], [61]. Our finding of hyperconnectivity of DMN is well supported by previous researches. We also identified a dysconnectivity network related to DAN and the visual cortex. The DAN is a task-positive network, which is engaged during externally directed attentional tasks and comprises functionally connected brain regions, including visual regions [62]. In MDD, the DAN is identified as abnormal in between-network connectivity with FN and DMN, which may reflect biases towards ruminative thoughts at the cost of attending to the external world [2].

It has been well demonstrated that MDD is related to the dysregulation of neural oscillatory synchrony, and our findings can provide references for the comprehensive information. In our study, the altered oscillations of the networks are notable in delta and alpha bands. It has been established that alpha synchronization plays a key global role in top-down network control [63]. The modulation of alpha oscillations has been demonstrated to be linked to the ability to shift and focus attention, and meet working memory and executive demands [64], [65]. In our study, the impaired networks of alpha dysregulation are related to the visual network (Figure 3I), TPN (Figure 3II), the SMN (Figure 3III), DMN (Figure 4III) and DAN (Figure 4IV), and those networks are well associated with attention regulation and working memory. Therefore, our results are consistent with previous findings. The dysregulation of delta oscillations has been related to various psychiatric disorders, including MDD [66]. Our results showed that the dysconnectivity networks regulated by delta oscillations are all related to the frontal network, including the prefrontal network (Figure 4I) and FTN (Figure 4II) and (Figure 3IV). From a review paper, Harmony concluded that the delta oscillations that originate in the frontal cortex might modulate the activity of neuronal networks that are distant from the frontal lobes, which can well support our findings [67].

Previous studies have shown that specific cell types and network structures are associated with the generation of different oscillations [68]. Our study well investigated the oscillatory networks, and the findings might reveal potential mechanisms in oscillatory synchrony between intrinsic cortical structures. Additionally, previous researches have provided much evidence that specific neurotransmitters can cause diverse effects on oscillatory synchrony across different brain areas, thus regulating various cognitive functions [68]–[71]. The results about altered synchronization via different oscillations could provide potential references in the neuropharmacology of MDD. The increasingly hot topic for MDD treatment using transcranial magnetic stimulation (TMS) has shifted the focus from individual brain regions to brain networks, because the effects of the stimulated brain region can be propagated to the connected network regions [72]–[74]. However, it is still unclear about the promising TMS targets and the corresponding distributed brain networks. Therefore, in the connectomics era of brain stimulation, identifying the connectivity-based TMS targets is crucial to improve clinical diagnosis. Our findings may be referred to reveal promising network targets.

We acknowledge some limitations and future directions of the current study. First, we only focus on the group differences in this study, and we assume the temporal, spectral and spatial consistency between each participant from the same group. However, the subject differences are important for clinical applications, and future work should take the subject differences into consideration. Second, we use the same anatomical image for each participant in the forward modeling due to lacking MRI data of the published data. For accurate source reconstruction, future work on data collection should include the anatomical MRI data. Third, the explanation for the oscillatory networks is limited because few studies link the functional networks with specific frequencies except predefined frequency bands. Modulation of the detailed frequencies for ICNs should be further studied. Fourth, the sliding window technique is used to measure the dynamic FC, which will limit the timescale of the FC fluctuations. The FC is dynamic in different timescales, and the corresponding

computational model should be designed in future work.

V. Conclusion

In this study, we proposed a novel framework based on coupled tensor decomposition to identify the oscillatory dysconnectivity networks in MDD using resting EEG. Highlighted from previous approaches, our method fully considered the high-dimensional structure of the data and the common and individual features of the oscillatory networks between the HC and MDD groups. We examined the dynamic networks modulated by specific frequencies and the hyper- and hypo-connectivity signatures in MDD. Our results are well explained by previous researches, thus providing valuable references for clinical diagnosis and treatment of MDD. The analysis pipeline is also applicable to other psychiatric disorders.

References

[1] Q. Gong and Y. He, "Depression, neuroimaging and connectomics: a selective overview," *Biological psychiatry*, vol. 77, no. 3, pp. 223–235, 2015.

[2] R. H. Kaiser, J. R. Andrews-Hanna, T. D. Wager, and D. A. Pizzagalli, "Large-scale network dysfunction in major depressive disorder: a meta-analysis of resting-state functional connectivity," *JAMA psychiatry*, vol. 72, no. 6, pp. 603–611, 2015.

[3] P. C. Mulders, P. F. van Eijndhoven, A. H. Schene, C. F. Beckmann, and I. Tendolkar, "Resting-state functional connectivity in major depressive disorder: a review," *Neuroscience & Biobehavioral Reviews*, vol. 56, pp. 330–344, 2015.

[4] G. C. O'Neill, P. Tewarie, D. Vidaurre, L. Liuzzi, M. W. Woolrich, and M. J. Brookes, "Dynamics of large-scale electrophysiological networks: A technical review," *Neuroimage*, vol. 180, pp. 559–576, 2018.

[5] S. Sadaghiani, M. J. Brookes, and S. Baillet, "Connectomics of human electrophysiology."

[6] M. Demirtaş, C. Tornador, C. Falcón, M. López-Solà, R. Hernández-Ribas, J. Pujol, J. M. Menchon, P. Ritter, N. Cardoner, C. Soriano-Mas *et al.*, "Dynamic functional connectivity reveals altered variability in functional connectivity among patients with major depressive disorder," *Human brain mapping*, vol. 37, no. 8, pp. 2918–2930, 2016.

[7] R. H. Kaiser, S. Whitfield-Gabrieli, D. G. Dillon, F. Goer, M. Beltzer, J. Minkel, M. Smoski, G. Dichter, and D. A. Pizzagalli, "Dynamic resting-state functional connectivity in major depression," *Neuropsychopharmacology*, vol. 41, no. 7, pp. 1822–1830, 2016.

[8] J. Wang, Y. Wang, H. Huang, Y. Jia, S. Zheng, S. Zhong, G. Chen, L. Huang, and R. Huang, "Abnormal dynamic functional network connectivity in unmedicated bipolar and major depressive disorders based on the triple-network model," *Psychological medicine*, vol. 50, no. 3, pp. 465–474, 2020.

[9] G. Li, Y. Liu, Y. Zheng, D. Li, X. Liang, Y. Chen, Y. Cui, P.-T. Yap, S. Qiu, H. Zhang *et al.*, "Large-scale dynamic causal modeling of major depressive disorder based on resting-state functional magnetic resonance imaging," *Human Brain Mapping*, vol. 41, no. 4, pp. 865–881, 2020.

[10] A. E. Whitton, S. Deccy, M. L. Ironside, P. Kumar, M. Beltzer, and D. A. Pizzagalli, "Electroencephalography source functional connectivity reveals abnormal high-frequency communication among large-scale functional networks in depression," *Biological Psychiatry: Cognitive Neuroscience and Neuroimaging*, vol. 3, no. 1, pp. 50–58, 2018.

[11] G. Buzsaki, *Rhythms of the Brain*. Oxford University Press, 2006.

[12] Y. Yan, T. Qian, X. Xu, H. Han, Z. Ling, W. Zhou, H. Liu, and B. Hong, "Human cortical networking by probabilistic and frequency-specific coupling," *NeuroImage*, vol. 207, p. 116363, 2020.

[13] A. A. Fingelkurts and A. A. Fingelkurts, "Altered structure of dynamic electroencephalogram oscillatory pattern in major depression," *Biological Psychiatry*, vol. 77, no. 12, pp. 1050–1060, 2015.

[14] A. A. Fingelkurts, A. A. Fingelkurts, H. Rytsälä, K. Suominen, E. Isometsä, and S. Kähkönen, "Impaired functional connectivity at eeg alpha and theta frequency bands in major depression," *Human brain mapping*, vol. 28, no. 3, pp. 247–261, 2007.

[15] D. Mantini, M. G. Perrucci, C. Del Gratta, G. L. Romani, and M. Corbetta, "Electrophysiological signatures of resting state networks in the human brain," *Proceedings of the National Academy of Sciences*, vol. 104, no. 32, pp. 13 170–13 175, 2007.

[16] K. Smitha, K. Akhil Raja, K. Arun, P. Rajesh, B. Thomas, T. Kapilamoorthy, and C. Kesavadas, "Resting state fmri: A review on methods in resting state connectivity analysis and resting state networks," *The neuroradiology journal*, vol. 30, no. 4, pp. 305–317, 2017.

[17] N. Leonardi, J. Richiardi, M. Gschwind, S. Simioni, J.-M. Annoni, M. Schluep, P. Vuilleumier, and D. Van De Ville, "Principal components of functional connectivity: a new approach to study dynamic brain connectivity during rest," *NeuroImage*, vol. 83, pp. 937–950, 2013.

[18] Y. Zhu, C. Zhang, H. Poikonen, P. Toiviainen, M. Huotilainen, K. Mathiak, T. Ristaniemi, and F. Cong, "Exploring frequency-dependent brain networks from ongoing eeg using spatial ica during music listening," *Brain Topography*, pp. 1–14, 2020.

[19] A. Cichocki, "Tensor decompositions: a new concept in brain data analysis?" *arXiv preprint arXiv:1305.0395*, 2013.

[20] J. Escudero, E. Acar, A. Fernández, and R. Bro, "Multiscale entropy analysis of resting-state magnetoencephalogram with tensor factorisations in alzheimer's disease," *Brain research bulletin*, vol. 119, pp. 136–144, 2015.

[21] A. G. Mahyari, D. M. Zoltowski, E. M. Bernat, and S. Aviyente, "A tensor decomposition-based approach for detecting dynamic network states from eeg," *IEEE Transactions on Biomedical Engineering*, vol. 64, no. 1, pp. 225–237, 2016.

[22] L. Spyrou, M. Parra, and J. Escudero, "Complex tensor factorization with parafac2 for the estimation of brain connectivity from the eeg," *IEEE Transactions on Neural Systems and Rehabilitation Engineering*, vol. 27, no. 1, pp. 1–12, 2018.

[23] W. Liu, X. Wang, T. Ristaniemi, and F. Cong, "Identifying task-based dynamic functional connectivity using tensor decomposition," in *International Conference on Neural Information Processing*. Springer, 2020, pp. 361–369.

[24] Y. Zhu, J. Liu, C. Ye, K. Mathiak, P. Astikainen, T. Ristaniemi, and F. Cong, "Discovering dynamic task-modulated functional networks with specific spectral modes using meg," *NeuroImage*, p. 116924, 2020.

[25] Y. Zhu, J. Liu, K. Mathiak, T. Ristaniemi, and F. Cong, "Deriving electrophysiological brain network connectivity via tensor component analysis during freely listening to music," *IEEE Transactions on Neural Systems and Rehabilitation Engineering*, 2019.

[26] B. Pester, C. Ligges, L. Leistritz, H. Witte, and K. Schiecke, "Advanced insights into functional brain connectivity by combining tensor decomposition and partial directed coherence," *PloS one*, vol. 10, no. 6, p. e0129293, 2015.

[27] E. Al-Sharoa, M. Al-Khassaweneh, and S. Aviyente, "Tensor based temporal and multilayer community detection for studying brain dynamics during resting state fmri," *IEEE Transactions on Biomedical Engineering*, vol. 66, no. 3, pp. 695–709, 2018.

[28] G. Hu, H. Li, W. Zhao, Y. Hao, Z. Bai, L. D. Nickerson, and F. Cong, "Discovering hidden brain network responses to naturalistic stimuli via tensor component analysis of multi-subject fmri data," *bioRxiv*, 2021.

[29] M. Roald, S. Bhinge, C. Jia, V. Calhoun, T. Adalı, and E. Acar, "Tracing network evolution using the parafac2 model," in *ICASSP 2020-2020 IEEE International Conference on Acoustics, Speech and Signal Processing (ICASSP)*. IEEE, 2020, pp. 1100–1104.

[30] X. Wang, W. Liu, P. Toiviainen, T. Ristaniemi, and F. Cong, "Group analysis of ongoing eeg data based on fast double-coupled nonnegative tensor decomposition," *Journal of neuroscience methods*, vol. 330, p. 108502, 2020.

[31] W. Liu, X. Wang, J. Xu, Y. Chang, T. Hamalainen, and F. Cong, "Identifying oscillatory hyperconnectivity and hypoconnectivity networks in major depression using coupled tensor decomposition," *bioRxiv*, 2021.

[32] H. Cai, Y. Gao, S. Sun, N. Li, F. Tian, H. Xiao, J. Li, Z. Yang, X. Li, Q. Zhao *et al.*, "Modma dataset: a multi-modal open dataset for mental-disorder analysis," *arXiv preprint arXiv:2002.09283*, 2020.

[33] A. Delorme and S. Makeig, "Eeglab: an open source toolbox for analysis of single-trial eeg dynamics including independent component analysis," *Journal of neuroscience methods*, vol. 134, no. 1, pp. 9–21, 2004.

[34] F. Tadel, S. Baillet, J. C. Mosher, D. Pantazis, and R. M. Leahy, "Brainstorm: a user-friendly application for meg/eeg analysis," *Computational intelligence and neuroscience*, vol. 2011, p. 8, 2011.

[35] M. Hassan, O. Dufor, I. Merlet, C. Berrou, and F. Wendling, "Eeg source connectivity analysis: from dense array recordings to brain networks," *PloS one*, vol. 9, no. 8, p. e105041, 2014.

[36] M. Bola and B. A. Sabel, "Dynamic reorganization of brain functional networks during cognition," *Neuroimage*, vol. 114, pp. 398–413, 2015.

[37] R. S. Desikan, F. Ségonne, B. Fischl, B. T. Quinn, B. C. Dickerson, D. Blacker, R. L. Buckner, A. M. Dale, R. P. Maguire, B. T. Hyman *et al.*, "An automated labeling system for subdividing the human cerebral

cortex on mri scans into gyral based regions of interest," *Neuroimage*, vol. 31, no. 3, pp. 968–980, 2006.

[38] C. J. Stam, G. Nolte, and A. Daffertshofer, "Phase lag index: assessment of functional connectivity from multi channel eeg and meg with diminished bias from common sources," *Human brain mapping*, vol. 28, no. 11, pp. 1178–1193, 2007.

[39] T. Womelsdorf, J.-M. Schoffelen, R. Oostenveld, W. Singer, R. Desimone, A. K. Engel, and P. Fries, "Modulation of neuronal interactions through neuronal synchronization," *science*, vol. 316, no. 5831, pp. 1609–1612, 2007.

[40] A. Cichocki, R. Zdunek, A. H. Phan, and S.-i. Amari, *Nonnegative matrix and tensor factorizations: applications to exploratory multi-way data analysis and blind source separation*. John Wiley & Sons, 2009.

[41] A. Cichocki, R. Zdunek, and S.-i. Amari, "Hierarchical als algorithms for nonnegative matrix and 3d tensor factorization," in *International Conference on Independent Component Analysis and Signal Separation*. Springer, 2007, pp. 169–176.

[42] A. Cichocki and A.-H. Phan, "Fast local algorithms for large scale nonnegative matrix and tensor factorizations," *IEICE transactions on fundamentals of electronics, communications and computer sciences*, vol. 92, no. 3, pp. 708–721, 2009.

[43] F. Lu, Q. Cui, X. Huang, L. Li, X. Duan, H. Chen, Y. Pang, Z. He, W. Sheng, S. Han *et al.*, "Anomalous intrinsic connectivity within and between visual and auditory networks in major depressive disorder," *Progress in Neuro-Psychopharmacology and Biological Psychiatry*, vol. 100, p. 109889, 2020.

[44] L. Wang, D. F. Hermens, I. B. Hickie, and J. Lagopoulos, "A systematic review of resting-state functional-mri studies in major depression," *Journal of affective disorders*, vol. 142, no. 1-3, pp. 6–12, 2012.

[45] M. Moreno-Ortega, J. Prudic, S. Rowny, G. Patel, A. Kangarlu, S. Lee, J. Grinband, T. Palomo, T. Perera, M. Glasser *et al.*, "Resting state functional connectivity predictors of treatment response to electroconvulsive therapy in depression," *Scientific reports*, vol. 9, no. 1, pp. 1–19, 2019.

[46] J. Brakowski, S. Spinelli, N. Dörig, O. G. Bosch, A. Manoliu, M. G. Holtforth, and E. Seifritz, "Resting state brain network function in major depression–depression symptomatology, antidepressant treatment effects, future research," *Journal of Psychiatric Research*, vol. 92, pp. 147–159, 2017.

[47] H. A. Eyre, H. Yang, A. M. Leaver, K. Van Dyk, P. Siddarth, N. S. Cyr, K. Narr, L. Ercoli, B. T. Baune, and H. Lavretsky, "Altered resting-state functional connectivity in late-life depression: a cross-sectional study," *Journal of affective disorders*, vol. 189, pp. 126–133, 2016.

[48] M. Martino, P. Magioncalda, Z. Huang, B. Conio, N. Piaggio, N. W. Duncan, G. Rocchi, A. Escelsior, V. Marozzi, A. Wolff *et al.*, "Contrasting variability patterns in the default mode and sensorimotor networks balance in bipolar depression and mania," *Proceedings of the National Academy of Sciences*, vol. 113, no. 17, pp. 4824–4829, 2016.

[49] F. Agosta, P. Valsasina, M. Absinta, N. Riva, S. Sala, A. Prelle, M. Copetti, M. Comola, G. Comi, and M. Filippi, "Sensorimotor functional connectivity changes in amyotrophic lateral sclerosis," *Cerebral cortex*, vol. 21, no. 10, pp. 2291–2298, 2011.

[50] G. Northoff, "How do resting state changes in depression translate into psychopathological symptoms? from 'spatiotemporal correspondence'to 'spatiotemporal psychopathology'," *Current opinion in psychiatry*, vol. 29, no. 1, pp. 18–24, 2016.

[51] D. Zhi, V. D. Calhoun, L. Lv, X. Ma, Q. Ke, Z. Fu, Y. Du, Y. Yang, X. Yang, M. Pan *et al.*, "Aberrant dynamic functional network connectivity and graph properties in major depressive disorder," *Frontiers in psychiatry*, vol. 9, p. 339, 2018.

[52] X. Wen, Y. Liu, P. Zhao, Z. Liu, H. Li, W. Li, Z. Zhu, and X. Wu, "Disrupted communication of the temporoparietal junction in patients with major depressive disorder," *Cognitive, Affective, & Behavioral Neuroscience*, pp. 1–21, 2021.

[53] K. M. Igelström and M. S. Graziano, "The inferior parietal lobule and temporoparietal junction: a network perspective," *Neuropsychologia*, vol. 105, pp. 70–83, 2017.

[54] J. Penner, E. A. Osuch, B. Schaefer, J. Theberge, R. W. Neufeld, R. S. Menon, N. Rajakumar, and P. C. Williamson, "Temporoparietal junction functional connectivity in early schizophrenia and major depressive disorder," *Chronic Stress*, vol. 2, p. 2470547018815232, 2018.

[55] D. Samson, I. A. Apperly, C. Chiavarino, and G. W. Humphreys, "Left temporoparietal junction is necessary for representing someone else's belief," *Nature neuroscience*, vol. 7, no. 5, pp. 499–500, 2004.

[56] A. Abu-Akel and S. Shamay-Tsoory, "Neuroanatomical and neurochemical bases of theory of mind," *Neuropsychologia*, vol. 49, no. 11, pp. 2971–2984, 2011.

[57] R. R. Davies, C. M. Kipps, J. Mitchell, J. J. Kril, G. M. Halliday, and J. R. Hodges, "Progression in frontotemporal dementia: identifying a benign behavioral variant by magnetic resonance imaging," *Archives of neurology*, vol. 63, no. 11, pp. 1627–1631, 2006.

[58] G. D. Rabinovici and B. L. Miller, "Frontotemporal lobar degeneration," *CNS drugs*, vol. 24, no. 5, pp. 375–398, 2010.

[59] F. Sambataro, N. D. Wolf, P. Giusti, N. Vasic, and R. C. Wolf, "Default mode network in depression: a pathway to impaired affective cognition?" *Clinical Neuropsychiatry*, vol. 10, no. 5, 2013.

[60] Y. I. Sheline, D. M. Barch, J. L. Price, M. M. Rundle, S. N. Vaishnavi, A. Z. Snyder, M. A. Mintun, S. Wang, R. S. Coalson, and M. E. Raichle, "The default mode network and self-referential processes in depression," *Proceedings of the National Academy of Sciences*, vol. 106, no. 6, pp. 1942–1947, 2009.

[61] M. G. Berman, S. Peltier, D. E. Nee, E. Kross, P. J. Deldin, and J. Jonides, "Depression, rumination and the default network," *Social cognitive and affective neuroscience*, vol. 6, no. 5, pp. 548–555, 2011.

[62] S. M. Szczepanski, M. A. Pinsk, M. M. Douglas, S. Kastner, and Y. B. Saalmann, "Functional and structural architecture of the human dorsal frontoparietal attention network," *Proceedings of the National Academy of Sciences*, vol. 110, no. 39, pp. 15 806–15 811, 2013.

[63] W. Klimesch, P. Sauseng, and S. Hanslmayr, "Eeg alpha oscillations: the inhibition–timing hypothesis," *Brain research reviews*, vol. 53, no. 1, pp. 63–88, 2007.

[64] A. F. Leuchter, I. A. Cook, A. M. Hunter, C. Cai, and S. Horvath, "Resting-state quantitative electroencephalography reveals increased neurophysiologic connectivity in depression," *PloS one*, vol. 7, no. 2, p. e32508, 2012.

[65] P. J. Uhlhaas and W. Singer, "Neural synchrony in brain disorders: relevance for cognitive dysfunctions and pathophysiology," *neuron*, vol. 52, no. 1, pp. 155–168, 2006.

[66] J. J. Newson and T. C. Thiagarajan, "Eeg frequency bands in psychiatric disorders: a review of resting state studies," *Frontiers in human neuroscience*, vol. 12, p. 521, 2019.

[67] T. Harmony, "The functional significance of delta oscillations in cognitive processing," *Frontiers in integrative neuroscience*, vol. 7, p. 83, 2013.

[68] G. G. Gregoriou, S. Paneri, and P. Sapountzis, "Oscillatory synchrony as a mechanism of attentional processing," *Brain research*, vol. 1626, pp. 165–182, 2015.

[69] M. Chalk, J. L. Herrero, M. A. Gieselmann, L. S. Delicato, S. Gotthardt, and A. Thiele, "Attention reduces stimulus-driven gamma frequency oscillations and spike field coherence in v1," *Neuron*, vol. 66, no. 1, pp. 114–125, 2010.

[70] G. Deco and A. Thiele, "Attention–oscillations and neuropharmacology," *European journal of neuroscience*, vol. 30, no. 3, pp. 347–354, 2009.

[71] A. A. Disney, C. Aoki, and M. J. Hawken, "Gain modulation by nicotine in macaque v1," *Neuron*, vol. 56, no. 4, pp. 701–713, 2007.

[72] R. F. Cash, A. Weigand, A. Zalesky, S. H. Siddiqi, J. Downar, P. B. Fitzgerald, and M. D. Fox, "Using brain imaging to improve spatial targeting of transcranial magnetic stimulation for depression," *Biological Psychiatry*, vol. 90, no. 10, pp. 689–700, 2021.

[73] C. Hawco, A. N. Voineskos, J. K. Steeves, E. W. Dickie, J. D. Viviano, J. Downar, D. M. Blumberger, and Z. J. Daskalakis, "Spread of activity following tms is related to intrinsic resting connectivity to the salience network: A concurrent tms-fmri study," *Cortex*, vol. 108, pp. 160–172, 2018.

[74] M. Tik, A. Hoffmann, R. Sladky, L. Tomova, A. Hummer, L. N. de Lara, H. Bukowski, J. Pripfl, B. Biswal, C. Lamm *et al.*, "Towards understanding rtms mechanism of action: stimulation of the dlpfc causes network-specific increase in functional connectivity," *Neuroimage*, vol. 162, pp. 289–296, 2017.